Article

Cell Reports

DNA Ligase IV Guides End-Processing Choice during Nonhomologous End Joining

Graphical Abstract

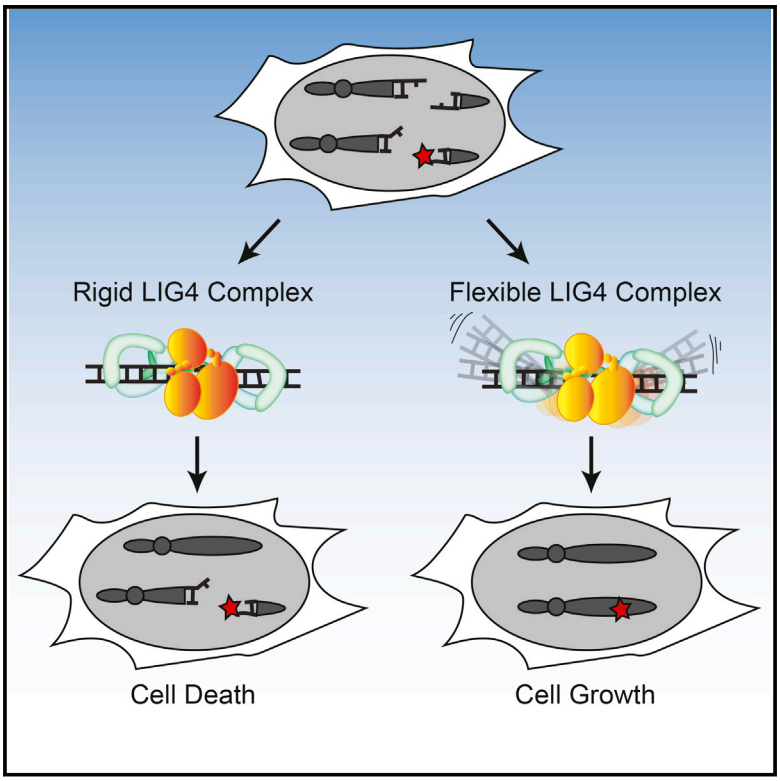

Authors

Michael P. Conlin, Dylan A. Reid, George W. Small, ..., Michael R. Lieber, Dale A. Ramsden, Eli Rothenberg

Correspondence

dale_ramsden@med.unc.edu (D.A.R.), eli.rothenberg@nyumc.org (E.R.)

In Brief

Conlin et al. show that, when DNA double-strand breaks have terminal mispairs or damage, an unstructured loop unique to DNA ligase IV allows for dynamic remodeling of the alignment and end repair; the loop is also required for cellular resistance to ionizing radiation.

Highlights

- Mobility of DNA ends aligned by NHEJ factors increases when ends are mispaired
- Increased end mobility requires insert1, a motif unique to the NHEJ ligase (LIG4)
- End mobilization is also essential for cellular repair of damaged and mispaired ends
- This mechanism explains the remarkable flexibility of NHEJ in the repair of diverse ends

Conlin et al., 2017, Cell Reports *20*, 2810–2819
September 19, 2017
http://dx.doi.org/10.1016/j.celrep.2017.08.091

OPEN ACCESS
CellPress

Cell Reports
Article

DNA Ligase IV Guides End-Processing Choice during Nonhomologous End Joining

Michael P. Conlin,[1,4] Dylan A. Reid,[2,4] George W. Small,[1] Howard H. Chang,[3] Go Watanabe,[3] Michael R. Lieber,[3] Dale A. Ramsden,[1,5,*] and Eli Rothenberg[2,5,6,*]

[1]Lineberger Comprehensive Cancer Center, Curriculum in Genetics and Molecular Biology, and Department of Biochemistry and Biophysics, University of North Carolina, Chapel Hill, NC 27599, USA
[2]Department of Biochemistry and Molecular Pharmacology, New York University School of Medicine, New York, NY 10016, USA
[3]University of Southern California Keck School of Medicine, Norris Comprehensive Cancer Center, Los Angeles, CA 90033, USA
[4]These authors contributed equally
[5]Senior author
[6]Lead Contact
*Correspondence: dale_ramsden@med.unc.edu (D.A.R.), eli.rothenberg@nyumc.org (E.R.)
http://dx.doi.org/10.1016/j.celrep.2017.08.091

SUMMARY

Nonhomologous end joining (NHEJ) must adapt to diverse end structures during repair of chromosome breaks. Here, we investigate the mechanistic basis for this flexibility. DNA ends are aligned in a paired-end complex (PEC) by Ku, XLF, XRCC4, and DNA ligase IV (LIG4); we show by single-molecule analysis how terminal mispairs lead to mobilization of ends within PECs and consequent sampling of more end-alignment configurations. This remodeling is essential for direct ligation of damaged and mispaired ends during cellular NHEJ, since remodeling and ligation of such ends both require a LIG4-specific structural motif, insert1. Insert1 is also required for PEC remodeling that enables nucleolytic processing when end structures block direct ligation. Accordingly, cells expressing LIG4 lacking insert1 are sensitive to ionizing radiation. Cellular NHEJ of diverse ends thus identifies the steps necessary for repair through LIG4-mediated sensing of differences in end structure and consequent dynamic remodeling of aligned ends.

INTRODUCTION

DNA double-strand breaks (DSBs) are genomic lesions that play an important role in human health and disease. They are frequently generated by exogenous damaging agents (e.g., ionizing radiation) or as programmed intermediates in meiosis and V(D)J recombination (Mehta and Haber, 2014). The ends generated by these biological sources of chromosome breaks are often "complex," with DNA helix-distorting nucleotide damage, mismatches, or chemical adducts that pose challenges to the ligases and polymerases needed for DSB repair (Breen and Murphy, 1995; Nitiss, 2009; Roth et al., 1992). This problem is especially relevant to the nonhomologous end joining (NHEJ) pathway, since, unlike other DSB repair pathways, these complex ends are not extensively resected prior to synthetic steps (polymerase and ligase activity; Waters et al., 2014a).

Ligation is the only essential step in NHEJ and is performed by one of the three mammalian ligases, DNA ligase IV (LIG4; Wilson et al., 1997). LIG4 is recruited to broken ends through participation in a complex of core NHEJ factors, including XRCC4, the Ku 70/80 heterodimer (Ku; Nick McElhinny et al., 2000), and XLF. This NHEJ core complex is sufficient to physically link a pair of broken ends together and can thus be termed the paired-end complex (PEC). The PEC is essential for repair of diverse end structures; for example, XLF is required both for stable PEC formation (Reid et al., 2015) and ligation of complex ends, but it only modestly affects ligation of ends with complementary termini (Andres et al., 2007; Gu et al., 2007; Tsai et al., 2007). Recent physical analyses of PECs indicate that they are highly dynamic (Reid et al., 2015) and that both the flexibility and stability of PECs can be modulated by ligation-compatible DNA end chemistry (Reid et al., 2017). However, it is unclear how differences in end structure trigger these changes in dynamics and whether these changes in dynamics impact cellular repair.

Here, we address this problem by assessing the impact of diverse end structures on in vitro functional assays, single-molecule analyses of end-pairing dynamics, and cellular repair and survival. We show that mismatches near strand-break termini trigger extensive PEC remodeling. Moreover, a separation-of-function mutation in LIG4 links this mispair-induced PEC remodeling to the sensing of these end structures by LIG4 and suggests that PEC remodeling is essential to the proficiency of cellular NHEJ in repairing these end structures.

RESULTS

LIG4^{WT} Is Specialized to Directly Ligate Mismatched or Damaged Ends

Activity of all three mammalian ligases requires the encircling of double-stranded DNA (dsDNA) at a strand break (Ellenberger and Tomkinson, 2008). Structural studies identified 6–10 amino acids inserted in LIG4 orthologs (residues 113–122 in human LIG4) relative to other eukaryotic ligases (Figures 1A and S1A; Ochi et al., 2013). This insert is located within the strand-break-bound ligase on the side of the double helix opposite of

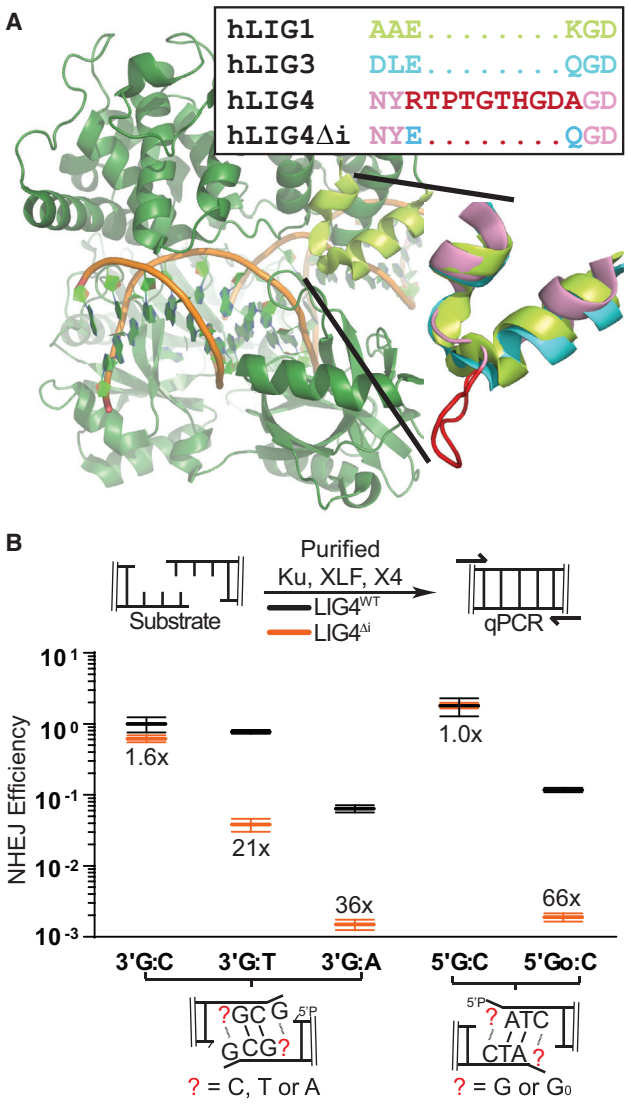

Figure 1. Effect of LIG4 Insert1 on NHEJ of Complex Ends In Vitro

(A) Structure of human LIG1 bound to DNA (PDB: 1X9N; green), with inset emphasizing sequence and structural alignments of human LIG1 α helices 5–6 to human LIG3 (PDB: 3L2P; blue) and human LIG4 (based on PDB: 3W1B; pink), with sequence and a modeled location of LIG4 insert1 (disordered in the 3W1B apoenzyme) in red.

(B) Ku, XLF, and either XRCC4-LIG4^{WT} (gray) or XRCC4-LIG4$^{\Delta i}$ (orange) were incubated with substrates containing different complementary (5′ G:C, 3′ G:C) or non-complementary (5′ GoxC, 3′ GxT, 3′ GxA) overhangs as noted. Joining efficiency is expressed as a fraction of the total junctions recovered using the 5′ G:C substrate with NHEJ reactions containing LIG4^{WT}. Ligation reactions were performed in triplicate, and the mean joining efficiencies are shown, along with the fold difference between LIG4^{WT} and LIG4$^{\Delta i}$ for each substrate. Error bars represent the range of observed values for each set of experiments.

the strand break and site of catalysis, suggesting a possible function specific to substrates with double-helix-distorting mispairs or damage. Consistent with this idea, we purified LIG4 with this element specifically deleted (LIG4$^{\Delta i}$) in a complex with XRCC4. We determined that insert1 had no significant impact on LIG4-XRCC4 intrinsic nick sealing activity (Figure S1B), DNA binding (Figure S1C), or ability to form a higher-order complex with the NHEJ core factors Ku and XLF on DNA (Figure S1D). In vitro NHEJ activity was also similar between LIG4$^{\Delta i}$ and LIG4^{WT} when ends had complementary overhangs (Figure 1B; 5′ G:C, 3′ G:C). In contrast, when ends had mispairs or damage at strand-break termini, in vitro NHEJ activity using LIG4$^{\Delta i}$ was reduced 21- to 66-fold relative to LIG4^{WT} (Figure 1B; 5′ GoxC, 3′ GxT, 3′ GxA). LIG4$^{\Delta i}$ is thus specifically defective in supporting in vitro NHEJ when substrates have helix-distorting 8-oxoguanine (G_o) damage or mispairs near strand termini.

Ends with mispaired nucleotides are critical NHEJ substrates that arise during V(D)J recombination and after nucleolytic processing of radiation-induced breaks. They also presumably act as a model for ends with other sources of helical distortion, including nucleotide damage. To validate this inference, we measured in vitro NHEJ of ends with 8-oxoguanine (Figure 1B; 5′ G_oxC), the most common form of oxidative base damage. NHEJ activity on this substrate was reduced over 50-fold with LIG4$^{\Delta i}$, which was comparable to the effect of a terminal G:A mispair. Therefore, insert1 is required for direct ligation of end structures with flanking helical distortions, whether the distortions are due to mispairs or nucleotide damage. To further explore the extent to which ligation of ends with terminal mispairs or damage is specific to wild-type LIG4, we generated a chimera (LIG^{3+4}) with all three LIG4 catalytic sub-domains replaced with the equivalent sub-domains from mammalian wild-type LIG3 (Figure S1E). Like LIG4$^{\Delta i}$, LIG^{3+4} physically associates with XRCC4 and was fully competent in Ku- and XLF-dependent ligation of ends with complementary overhangs. However, end joining with this chimera was even more sensitive than LIG4$^{\Delta i}$ to terminal nucleotide damage (activity reduced more than 100-fold, relative to LIG4^{WT}; Figure S1E). This result is consistent with the argument that LIG4 is unique among mammalian ligases in its ability to repair damaged termini. Additionally, the impact of LIG4$^{\Delta i}$ on repair of damaged ends is less severe than that of the LIG^{3+4} chimera, suggesting that insert1 is not entirely responsible for the unique ability of LIG4 to tolerate mispairs and damage. We therefore sought to use the LIG4$^{\Delta i}$ separation-of-function mutation to investigate both the mechanistic basis for the unique ability of NHEJ to tolerate helix-distorting mispairs or damage at the ligation step, as well as its significance to cellular double strand break repair.

Dynamic Re-alignment of Mismatched Ends Is Required for Their Ligation

We previously described a single-molecule fluorescence resonance energy transfer (smFRET) assay that reports on pairing of DNA ends as mediated by a complex of Ku, XRCC4, LIG4, and XLF (Reid et al., 2015, 2017). These PECs are apparent as FRET pairs generated when a Cy3-labeled donor dsDNA fragment in solution stably associates with a Cy5-labeled acceptor dsDNA fragment immobilized on a surface (Figure 2A). In accord with the in vitro ligation assay, LIG4$^{\Delta i}$ and LIG4^{WT} similarly promote stable PEC formation when ends have complementary 4-nt overhangs (G:C; Figure 2B). In contrast, pairing of overhangs with 3′ terminal G:T mismatches is significantly reduced when comparing LIG4$^{\Delta i}$ to LIG4^{WT}; this reduced pairing

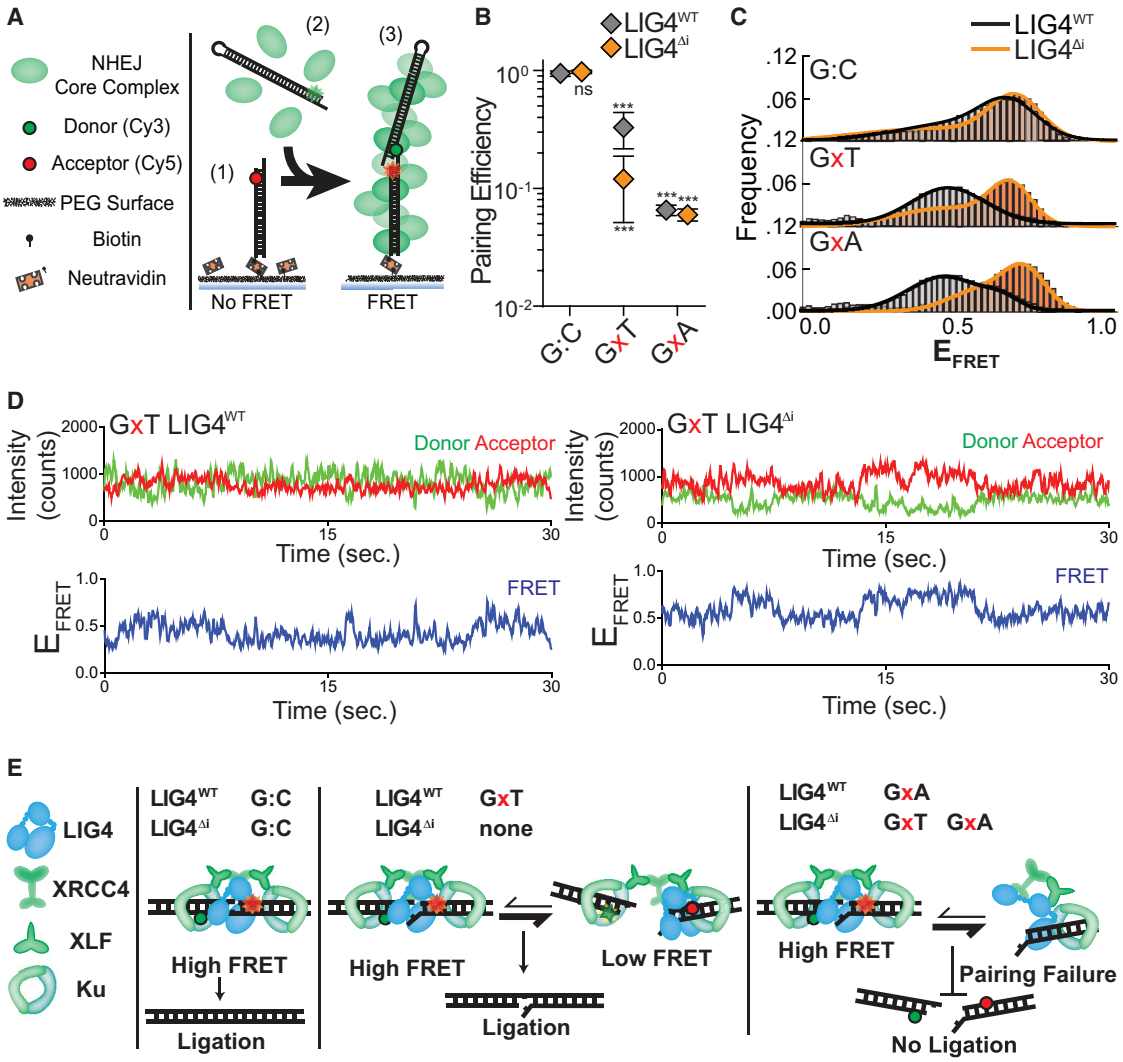

Figure 2. Effect of Complex End Structures on Pairing Dynamics of Single-Molecule Complexes with LIG4^{WT} or LIG4$^{\Delta i}$

(A) smFRET NHEJ assay: (1) dsDNA with a Cy5 acceptor is tethered to a bitonylated PEG surface via a biotin-neutravadin linkage, (2) dsDNA with a Cy3 donor and NHEJ proteins (green) are added to the chamber, and (3) ends are paired and FRET is observed.

(B) Quantitation of pairing efficiency of ends with complementary (G:C) or mismatched (GxT, GxA) overhangs by Ku, XLF, XRCC4, and either LIG4^{WT} (gray) or LIG4$^{\Delta i}$ (orange). Error bars represent SEM for 3 experiments. Means were assessed by two-way ANOVA as significantly different from control (LIG4^{WT} on G:C substrate) with confidence $p < 0.001$ (***).

(C) Histograms of observed E_{FRET} for PECs formed as in (B).

(D) Representative smFRET trajectory for LIG4^{WT} and LIG4$^{\Delta i}$ PECs formed with GxT ends demonstrating altered transition frequency and FRET states.

(E) LIG4^{WT} enables PECs to oscillate between high and low E_{FRET} states in response to distortions, and this flexibility is essential for joining distorted breaks.

efficiency represents a diminished proportion of DNA ends associated in the PEC. The formation of PECs is even less efficient when termini have a bulkier purine:purine G:A mismatch but is similarly inefficient for both LIG4^{WT} and LIG4$^{\Delta i}$ (Figure 2B). PECs thus form less efficiently with increasing terminal helical distortion, and PECs formed with LIG4$^{\Delta i}$ are more sensitive to this challenge.

Changes in FRET efficiency (E_{FRET}) reflect dynamic repositioning of DNA ends relative to each other within individual PECs (Reid et al., 2015, 2017). When using complementary ends (3′ G:C; Figure 2C), E_{FRET} distributions were not significantly different when comparing PECs formed with LIG4^{WT} (black line) versus LIG4$^{\Delta i}$ (orange line). LIG4$^{\Delta i}$ PECs also had similar FRET distributions when ends had terminal mispairs (Figure 2C); importantly, LIG4^{WT} PECs formed on ends with mispaired termini more often had lower E_{FRET} (DNA labels located further apart; Figure 2C, black lines for G:A and G:T mispairs) and consequently overall wider distributions of E_{FRET} (Figures 2C and S2A) when compared to paired termini (G:C). Ends with terminal distortions thus trigger PECs to sample a wider variety of end-alignment configurations to remain efficiently paired, but only when using LIG4^{WT}.

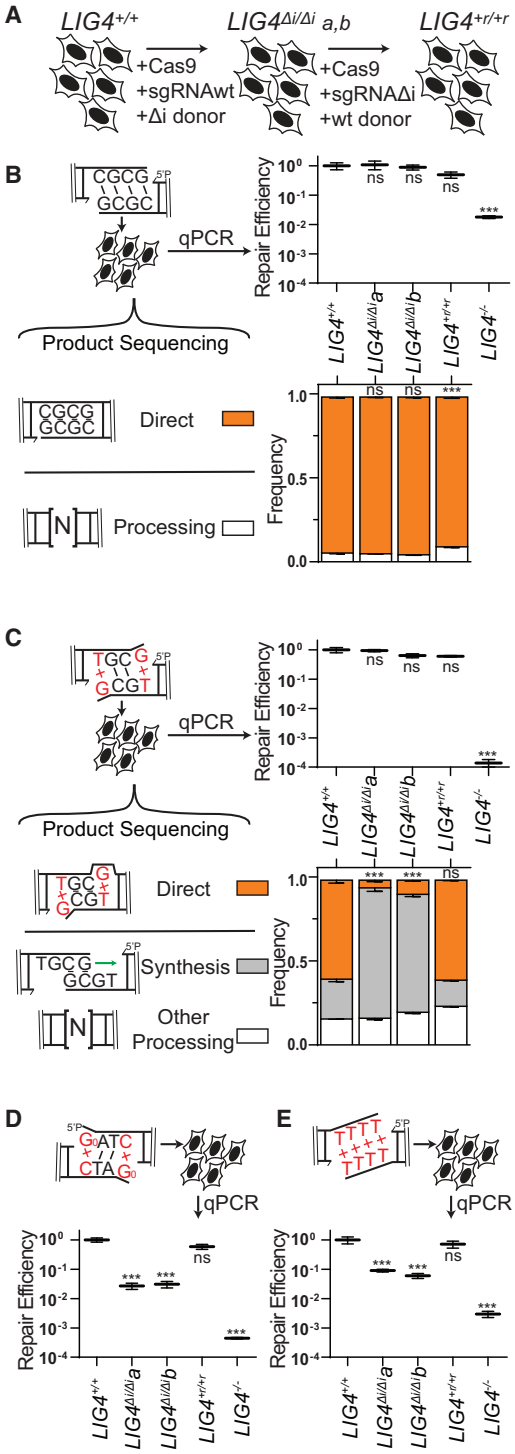

Examination of smFRET trajectories from individual PECs also shows the transition frequency between FRET states increases when comparing LIG4^{WT} and LIG4$^{\Delta i}$ (Figures 2D and S2C). We quantified this difference by using autocorrelation of individual FRET trajectories to calculate the average transition times ("lag times" [τ]) between FRET states. For ends with G:T mismatches, these were ~2-fold lower for PECs formed with LIG4^{WT} than for PECs formed with LIG4$^{\Delta i}$ (Figure S2B; Reid et al., 2017). These values are then used to calculate the relative stability of the DNA ends in the PECs (Figure S2C). From these calculated end stabilities, we can infer that LIG4^{WT} PECs have lower energetic barriers in assuming new conformations than LIG4$^{\Delta i}$ PECs, but again only when ends have terminal mismatches.

PECs containing LIG4$^{\Delta i}$ and mispaired ends are thus formed less efficiently (Figure 2B) and even when formed do not acquire the high degree of conformational plasticity observed when PECs are formed with LIG4^{WT} (Figures 2C, 2D, S2D, and S2E). We argue the inability of LIG4$^{\Delta i}$ to allow for mispair-induced PEC remodeling accounts for its specific defect in direct ligation of such end structures (Figure 1B). There are also limits to the extent to which remodeling enables ligation, as even LIG4^{WT} is inefficient in joining ends with bulky G:A mismatches (Figure 1B). PECs formed with paired termini favor a narrow distribution of high FRET end alignments that more closely resemble FRET distributions observed with products of ligation (Reid et al., 2015); these alignments thus likely directly juxtapose strand-break termini in anticipation of catalytic steps ("pre-catalytic"; Figure 2E). We attribute the LIG4^{WT}-specific, insert1-dependent flexibility in accommodation of mispaired termini to a favoring of end alignments that both have lower FRET (more distally located labels) and are more dynamic. These more dynamic and lower FRET PECs ("remodeling" PECs) may be catalytically incompetent, but they allow for iterative attempts at the now transient (but occasionally catalytically competent) high-FRET intermediate (Figure 2E).

Cellular NHEJ of Complex Ends Requires Remodeling of the PEC

We next addressed whether the differences in PEC flexibility described above significantly impact cellular NHEJ. We employed scar-free gene targeting to exchange *LIG4*^{WT} for *LIG4*$^{\Delta i}$ alleles within the native *LIG4* locus of a human cell line (Figure 3A). We independently generated two such cell lines (*LIG4*$^{\Delta i/\Delta i}$a and *LIG4*$^{\Delta i/\Delta i}$b) and confirmed they express only LIG4$^{\Delta i}$ from endogenous loci (Experimental Procedures; Figures S3A and S3B). We then generated a cell line by another round of gene targeting where the *LIG4* locus of *LIG4*$^{\Delta i/\Delta i}$a was reverted back to wild-type sequence (*LIG4*$^{+r/+r}$) as a means of assessing the effects of possible off-target mutations incurred in the

Figure 3. Effect of LIG4 Insert1 on Cellular Joining of Complex End Structures

(A) Cells were engineered to express LIG4$^{\Delta i}$ from the native LIG4 locus by CRISPR/Cas9-based gene targeting, and the LIG4$^{\Delta i}$-a clone was then reverted back to wild-type (*LIG4*$^{+r/+r}$) by a second round of gene targeting.

(B–E) Substrates with varied end structures were introduced in the cell types described in (A). Joining efficiency was assessed by qPCR and product structure by sequencing or diagnostic restriction digestion and defined as directly ligated or ligated after end processing as noted. Cellular NHEJ was assessed for complementary ends (B), ends with 3′ G:T terminal mismatches (C), ends with 5′ terminal 8-oxoguanine (Go; product structures reported in Figure S3D) (D), and ends with fully non-complementary overhangs (product structures reported in Figure S3E) (E). Error bars represent SEM for 3 experiments. Means of linearized qPCR data and direct joining products were assessed by one-way ANOVA as significantly different from control (*LIG4*$^{+/+}$ cells) with confidence $p < 0.001$ (***) or not significantly different (ns).

original round of gene targeting (Figures 3A, S3A, and S3B). Both *LIG4*$^{\Delta i/\Delta i}$ subclones acted equivalently in functional assays below. Similarly, results using parental wild-type cells (*LIG4*$^{+/+}$) matched those from the *LIG4*$^{+r/+r}$ reversion, confirming the differences observed in the *LIG4*$^{\Delta i/\Delta i}$ cells could be attributed to the 8-amino-acid deletion.

DSB substrates with varied end structures were introduced into these cells, after which efficiency of repair was determined by qPCR and product structures were characterized by high-throughput sequencing. In accord with in vitro results, ends with complementary overhangs were efficiently joined almost entirely by direct ligation in both wild-type and *LIG4*$^{\Delta i/\Delta i}$ cells (Figure 3B). Also in accord with in vitro data, ends with terminal G:T mispairs were efficiently repaired by direct ligation (accounts for 60% of all repair) in both *LIG4*$^{+/+}$ and *LIG4*$^{+r/+r}$ cells, while this class of product is rarely (<10%) seen in *LIG4*$^{\Delta i/\Delta i}$ clones (Figure 3C). Instead, repair in *LIG4*$^{\Delta i/\Delta i}$ cells typically requires re-alignment of overhangs and gap-repair synthesis prior to ligation of the now "sticky" end. This alternate pathway is sufficient to fully compensate for the inability of LIG4$^{\Delta i}$ to directly ligate terminal mispairs, since overall joining efficiency was comparable for *LIG4*$^{+/+}$ versus *LIG4*$^{\Delta i/\Delta i}$ cells. Considering repair of ends with bulkier G:A mispairs, both wild-type and *LIG4*$^{\Delta i/\Delta i}$ cells rely on this compensating pathway (Figure S3C), consistent with in vitro observations that neither LIG4^{WT} nor LIG4$^{\Delta i}$ can ligate this substrate in the absence of end processing. Repair of NHEJ substrates was severely reduced in *LIG4*$^{-/-}$ cells (Figure 3C; ~0.0005 products per cell) to the extent that we could not recover sufficient repair products to accurately assess product spectra.

Additional substrates were introduced into cells to assess whether barriers to mispair tolerance are routinely bypassed by cellular end processing. Similar to 3′ G:T mispairs, ends with 5′ G_o terminal damage are primarily repaired by direct ligation in *LIG4*$^{+/+}$ cells. Importantly, joining of 5′ G_oxC in *LIG4*$^{\Delta i/\Delta i}$ cells is over 10-fold less efficient (Figure 3D), even though what little repair does occur is processing dependent (Figure S3D). We also investigated cellular NHEJ of end structures with entirely non-complementary overhangs (TTTT). Joining efficiency was again severely reduced in *LIG4*$^{\Delta i/\Delta i}$ cells relative to wild-type cells (Figure 3D). For this substrate, the rare products recovered from *LIG4*$^{\Delta i/\Delta i}$ cells only subtly differed from wild-type controls in terms of junction structure (Figure S3E). Thus, in contrast to previously tested substrates (Figure 3C), end processing was not sufficient to rescue repair of TTTT and 8-oxoguanine substrates in *LIG4*$^{\Delta i/\Delta i}$ cells. We initially linked LIG4^{WT} PEC flexibility only to the ability of cellular NHEJ to directly ligate ends with terminal mispairs (Figures 1, 2, and 3C); these latter results identify additional important contributions to cellular NHEJ associated with end processing.

Role for PEC Remodeling in Guiding End-Processing Choice during Cellular NHEJ

We generated the substrate "EC1" (embedded complementarity 1) to further explore the relationships among PEC flexibility, cellular end processing, and ligation. EC1 has long (10-nt) non-complementary overhangs that can plausibly be aligned to juxtapose mispaired 3′OH:5′P termini in anticipation of direct ligation (Figure 4A). Alternatively, EC1 can be re-aligned to pair a complementary sequence embedded within the overhang, where unpaired tails are a presumptive substrate for nucleolytic end processing. These two alignments are readily distinguished by smFRET (Figure S4A); PECs formed with a control substrate (with fully complementary 10-nt overhangs) had low E_{FRET} ranges, as expected for EC1 alignments that juxtapose 3′OH:5′P termini (green lines), while PECs formed with 4-nt complementary overhangs had a clearly distinct population of high E_{FRET} (blue lines), as expected for EC1 alignments that pair embedded complementary sequence. Analysis of individual smFRET trajectories of PECs formed with EC1 and NHEJ core factors identified a much larger than typical fraction of transient complexes (lifetimes <5 s; Figure 4B). Transient PECs had two distinct populations of E_{FRET} distributions, each roughly corresponding to the two alignment classes predicted above (Figure 4C). Long-lived PECs (persistent) favor only the high E_{FRET} state, but sample both a wider range of alignment configurations (Figure 4C) and are more dynamic (have lower energetic barriers to transition; Figure S4B) than PECs formed with complementary overhangs. To further address if the persistent PECs frequently involve pairing at embedded complementary sequence (as suggested by comparison to substrate standards; Figure 4C) we used a substrate where the complementary sequence was both reduced and re-located ("EC2"). As expected, PECs formed less efficiently with EC2 (Figure S4C), and when formed had mostly lower E_{FRET} (Figure S4D). Importantly, LIG4$^{\Delta i}$ was largely unable to form PECs with the EC1 substrate (Figure 4D), and the rare PECs that do form primarily have intermediate E_{FRET} states that are inconsistent with either alignment (Figure S4E). Therefore, only LIG4^{WT} effectively promotes end-pairing of this substrate. Moreover, PECs formed with LIG4^{WT} that juxtapose strand termini were "filtered out"; only the most plausibly productive alignments, i.e., those that could lead to ligation after nucleolytic end processing, were stable (Figure 4C).

We next assessed how the EC1 substrate was resolved by cellular NHEJ. Nearly all products (>99%) were indeed consistent with ligation after nuclease activity, with the dominant product guided by the alignment at embedded complementary sequence also favored in smFRET analysis (Figure S4F). By comparison, direct ligation of EC1 accounted for less than 0.1% of all cellular repairs. Importantly, joining efficiency of this substrate was reduced over 60-fold in *LIG4*$^{\Delta i/\Delta i}$ cells relative to *LIG4*$^{+/+}$ cells (Figure 4E), even though *LIG4*$^{\Delta i/\Delta i}$ cells are fully proficient at ligating the inferred product of alignment-guided nuclease activity (a 4-bp complementary overhang; Figure 3B). This result suggests that for this substrate, LIG4$^{\Delta i}$ fails to efficiently mediate repair, because it is defective at a step that occurs before ligation—specifically, stable accommodation of end-alignments required for nucleolytic end processing (Figure 4D).

Resistance to Ionizing Radiation Requires Tolerance of Complex Ends by LIG4

LIG4^{WT} thus uniquely accommodates diverse end structures during end pairing. However, there is wide variation in how this flexibility impacts cellular NHEJ. Depending on the starting end structure, it can be dispensable (Figures 3B and S3C), alter product spectra (Figure 3C), or be critical for efficient repair

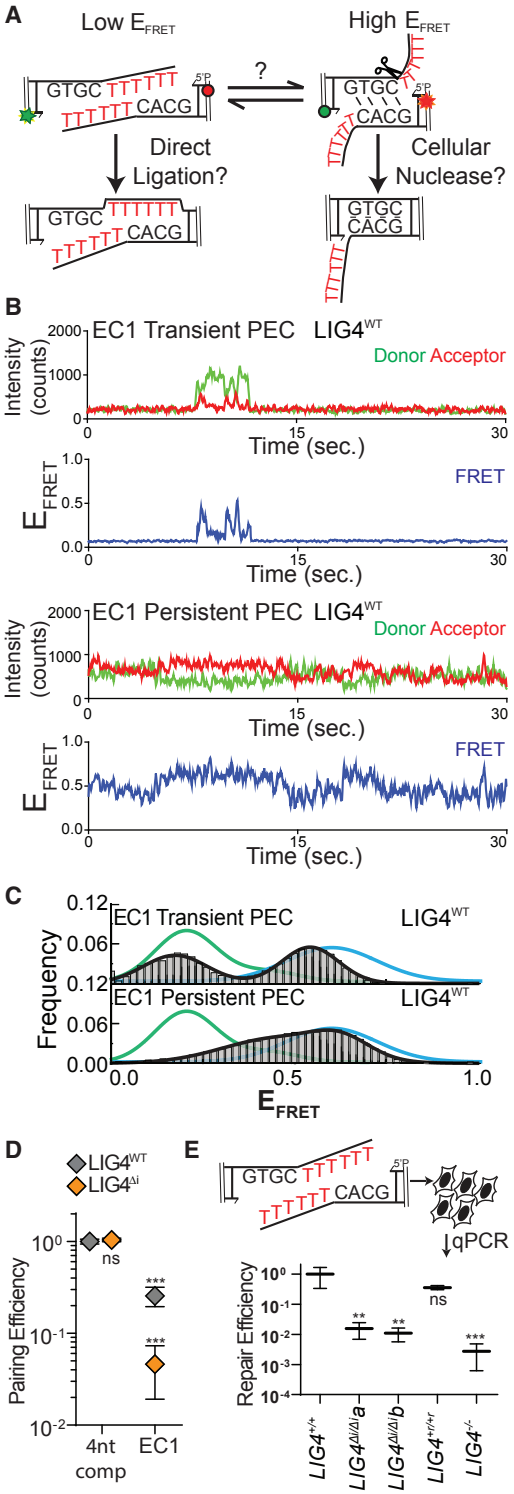

Figure 4. Effect of PEC Flexibility on Nucleolytic End Processing

(A) A substrate was designed with embedded complementarity (EC1) that can be aligned in a high-FRET conformation guided by base pairing (a presumptive nuclease substrate) or in a low-FRET conformation with juxtaposition of 5′ and 3′ termini.

(B) Representative smFRET trajectories for transient (short-lived; <30 s) and persistent (long-lived; ≥30 s) PECs formed with the EC1 substrate.

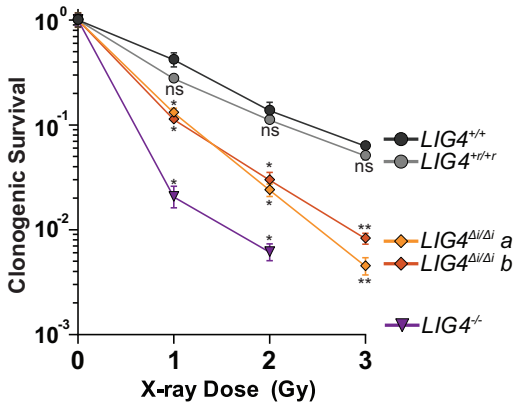

Figure 5. Effect of LIG4 Insert1 on Cellular Sensitivity to Ionizing Radiation

Cells were exposed to the indicated doses of X-rays and assessed for colony formation. Data represent the mean and SD of 3 experiments. Mean surviving fractions were assessed by one-way ANOVA as significantly different from control (*LIG4*$^{+/+}$ cells) independently for each dose with confidence $p < 0.05$ (*), $p < 0.01$ (**), or not significantly different (ns).

(Figures 3D, 3E, and 4E). We therefore addressed the extent to which the inability of LIG4 to tolerate structural diversity impacts cell growth and survival after ionizing radiation. Using both standard colony-forming assays and real-time imaging of cell growth, *LIG4*$^{+/+}$ and *LIG4*$^{+r/+r}$ cells were similarly resistant to increasing dose of ionizing radiation. By comparison, *LIG4*$^{\Delta i/\Delta i}$ cells were radiosensitive to a degree intermediate between *LIG4*$^{+/+}$ and *LIG4*$^{-/-}$ cells (Figures 5 and S5), a result strikingly similar to joining efficiencies described for the majority of substrates with complex ends (Figures 3D, 3E, and 4E). In contrast with ionizing radiation, *LIG4*$^{\Delta i/\Delta i}$ and *LIG4*$^{+/+}$ cells are equally resistant to etoposide (Figure S5). This is consistent with specific requirement for insert1 in repair of ends with mispairs or damage, since etoposide-induced breaks can be processed by tyrosine phosphodiesterase 2 such that overhangs are undamaged and fully complementary (Gómez-Herreros et al., 2013). These results show that the ability of LIG4 to sense distortions facilitates cell survival following treatment with ionizing radiation.

DISCUSSION

Repair by NHEJ implicitly requires the pairing together of broken chromosome ends. A complex of Ku, XRCC4, DNA ligase IV, and XLF (PEC) is necessary and sufficient for this purpose (Reid et al.,

(C) Histograms of E_{FRET} of transient (top) or persistent (bottom) LIG4^{wt} PECs formed on the EC1 substrate (black), compared to FRET standards with complementary overhangs either 4 nt (blue) or 10 nt (green) in length.

(D) Quantitation of pairing efficiency of EC1 substrate by LIG4^{WT} (gray) or LIG4$^{\Delta i}$ (orange). Error bars represent SEM for 3 experiments. Means were assessed for significance as in Figure 2B with confidence $p < 0.001$ (***) or not significantly different (ns).

(E) The EC1 substrate was transfected into cells and repair efficiency was quantitated by qPCR. Error bars represent SEM for 3 experiments. Linearized means were assessed for significance as in Figures 3B–3E with confidence $p < 0.01$ (**), $p < 0.001$ (***), or not significantly different (ns).

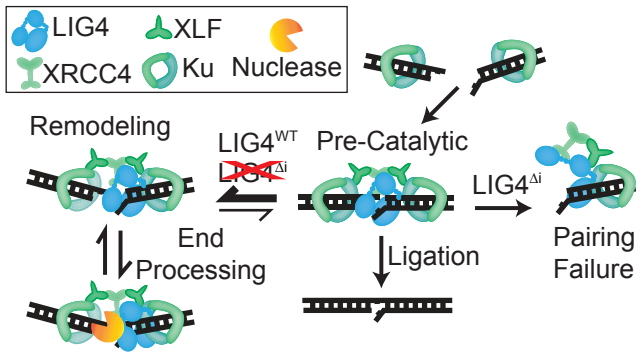

Figure 6. Sensing of Differences in End Structure by LIG4 Guides Repair

Model for LIG4-dependent remodeling of PECs in response to complex ends.

2015). Here, we describe dynamic changes in this complex that are triggered by differences in end structure and show that this response is essential for efficient cellular repair.

Mechanistic Basis for Repair of Complex Ends by NHEJ

Ends with complementary (sticky) overhangs are aligned efficiently and with little mobility, to the extent that pairing E_{FRET} more closely resemble the narrow distributions observed in products of ligation (Reid et al., 2015), relative to other end structures tested here. We suggest these PECs describe pre-catalytic end alignments, where strand break termini are directly juxtaposed in anticipation of ligase-mediated catalytic steps (Figure 6). In contrast, ends with helix-distorting mispairs or damage near strand termini (complex ends) induce the sampling of a much wider variety of alignment configurations, most or all of which no longer juxtapose strand termini.

We use a LIG4 separation-of-function mutation ($LIG4^{\Delta i}$) to identify an essential role for this second, more dynamic remodeling class of PECs in cellular NHEJ for the repair of complex ends. We show $LIG4^{\Delta i}$ is specifically unable to accommodate PEC remodeling in response to complex ends. As a consequence, PECs formed with $LIG4^{\Delta i}$ are unable to directly ligate such substrates, but are also, with a rare exception (Figure 3C), unable to couple ligation to end processing when end complexity is sufficient to block direct ligation.

Notably, the exceptions are restricted to contexts where alignment-directed synthesis generates a fully complementary 6-nt overhang, a substrate expected to be especially permissive for the ligation step.

By comparison, insert1 is dispensable for the XLF-, XRCC4-, and Ku-dependent alignment of ends with complementary overhangs, as well as catalytic activity on this conventional ligase substrate. Moreover, a chimeric ligase with all three LIG4 catalytic subdomains replaced with LIG3 counterparts is equally effective in ligation of sticky ends (and is similarly stimulated by Ku and XLF) but is even less able to repair complex ends. Prior work emphasized the importance of a variety of NHEJ factors, including PAXX (Ochi et al., 2015; Xing et al., 2015), end-processing factors (Chang et al., 2016; Ma et al., 2002; Pryor et al., 2015), and especially the end-bridging filament of XRCC4-XLF (Andres et al., 2012; Gu et al., 2007; Roy et al., 2015) in repairing complex breaks. Indeed, we previously reported that these filaments form on bleomycin-induced DSBs and orchestrate their repair (Reid et al., 2015). Here, we identify a critical role for specialization of LIG4 catalytic subdomains in repair of complex ends and show this role is attributable to insert1-dependent PEC remodeling.

How does insert1 contribute to PEC remodeling? The three subdomains of eukaryotic ligases are extended in the absence of DNA ("open" conformation) and engage substrates by forming a ring around dsDNA ("closed" conformation; Cotner-Gohara et al., 2010; Nair et al., 2007; Pascal et al., 2004). In the closed conformation, the central catalytic subdomain is bound to strand-break termini, while insert1 is located in the N-terminal subdomain on the opposite side of the double helix (Ochi et al., 2013). Though not resolved in current apo-enzyme crystal structures, its location suggests that insert1 helps LIG4 maintain a closed conformation, either by stabilizing the ring-closing interactions between N- and C-terminal catalytic subdomains or by interacting with DNA (Ochi et al., 2012). We suggest that stable end pairing is dependent on LIG4 maintaining a closed conformation, even if LIG4 can directly interact with only the 5′ phosphate side of a strand break ("half-site" binding). $LIG4^{\Delta i}$ instead transitions to an open conformation in this context (like conventional ligases), which leads to failure of end pairing.

Significance of LIG4 Sensing Complex Ends

Prior work indicates that LIG4 has functions in NHEJ distinct from the ligation step, most clearly in promoting end pairing (Budman et al., 2007; Cottarel et al., 2013; Davis et al., 2008; Reid et al., 2015, 2017). Data presented here identify a much more sophisticated function. Differences in how LIG4 catalytic domains interact with different end structures trigger dramatic changes in the dynamics of the entire PEC (i.e., including Ku, XRCC4, and XLF paired ends), and these altered dynamics determine the steps taken to complete repair. This role is distinct from critical LIG4 roles in catalysis and end pairing, since both of the latter functions are fully intact in PECs formed with $LIG4^{\Delta i}$. LIG4 can thus be identified as the PEC "sensor," helping tailor the path to repair as is appropriate to end structure, possibly even to the extent that how LIG4 interacts with aligned ends may dictate the identity of the end-processing factor that next engages the end.

Inhibitors of LIG4 are being explored for their potential to sensitize tumors to radiation therapy (Tomkinson et al., 2013). Here, we identify a role of LIG4 that is specific to the ability of cells to repair complex damage, identify a structural element required for this role, and show that deletion of this element leads to cellular sensitivity to ionizing radiation. Since this structural element is unique to LIG4 and required for radioresistance, it presents a promising therapeutic target, as it is less likely to engender the off-target effects observed with current LIG4 inhibitors (Greco et al., 2016).

EXPERIMENTAL PROCEDURES

DSB Substrates

DSB substrates were made by ligating the 15- to 30-bp double-stranded oligonucleotide "caps" described in Table S1 to a 285-bp PCR-generated common

DNA "core" segment that had been digested with BsaI to generate appropriate sticky ends. Substrates were purified with the QiaQuick PCR purification kit (QIAGEN), 5′ phosphorylated with T4 polynucleotide kinase (NEB), and substrate assembly validated by gel electrophoresis.

DNA Constructs and Protein Purification

Constructs for expression after baculovirus delivery of human Ku, XLF, XRCC4, and LIG4^{WT} into Hi-5 insect cells have been previously described (Nick McElhinny et al., 2005; Roberts et al., 2010). LIG4$^{\Delta i}$ was generated by modifying LIG4^{WT} as noted in Figure 1A and validated by sequencing. The LIG^{3+4} chimera was generated by replacing amino acids 1–638 of LIG4^{WT} with a fusion of amino acids 170–862 of human LIG3 to the linker (GGGGS)x3 (Genewiz). Cell pellets were extracted, lysed by sonification, and purified by sequential chromatography on Histrap and MonoQ columns (GE Biosciences). Figure 1A structures were prepared in Pymol and include hLIG1 (PDB: 1X9N; Pascal et al., 2004), hLIG3 (PDB: 3L2P; Cotner-Gohara et al., 2010), and hLIG4 (PDB: 3W1B; Ochi et al., 2013), with disordered insert1 modeled by the SWISSmodel server (Biasini et al., 2014).

In Vitro Joining Assays

NHEJ reactions were initiated by incubating 2 nM DSB substrates, 25 nM Ku, 40 nM XLF, and 40 nM XRCC4-LIG4 in a buffer with 25 mM Tris (pH 7.5), 100 μM EDTA, 1 mM DTT, 5 mM MgCl, 100 μM ATP, 150 mM KCl, 8.5% polyethylene glycol 3000, and 100 ng supercoiled plasmid DNA. Reactions were carried out for 10 min at 37°C and stopped with 0.1% SDS and 20 mM EDTA. Repair products were purified by phenol-chloroform extraction and recovery was measured by real-time PCR (qPCR) using a QuantStudio 6 system (Applied Biosciences), primers that amplify head-to-tail junctions (Table S1), and VeriQuest SYBR Green master mix (Affymetrix). The relative numbers of molecules recovered were quantified by a well-characterized qPCR assay (Pryor et al., 2015; Waters et al., 2014b).

For nick-sealing assays, a 5′Cy5-labeled, nicked 41-bp substrate was generated by annealing three oligonucleotides (Table S1). 5 nM substrate was incubated with XRCC4-LIG4 at 37°C, and products were characterized by denaturing PAGE. Wild-type XRCC4-LIG4 was titrated to determine that 0.5 nM ligase (1:10 enzyme/substrate) generates sub-saturating (19%–21%) amounts of nick sealing in 10 min, after which reactions were carried out under these conditions in triplicate to generate data presented in Figure S1B. Reaction velocity was determined by quantifying band intensities using ImageJ software.

EMSA

Substrates for the electrophoretic mobility shift assay (EMSA) were generated by annealing oligonucleotides (Table S1) to produce a Cy5-labeled 15-bp substrate to assess DSB end binding (Figure S1C), as well as a Cy5-labeled, 60-bp substrate to assess complex formation (Figure S1D). To assess intrinsic end binding, the 15-bp substrate was incubated at 10 nM with 125, 250, or 500 nM XRCC4-LIG4. For complex formation, the 60-bp substrate was incubated at 10 nM with 2 nM Ku, 40 nM XLF, and 40 nM XRCC4-LIG4. These samples were incubated for 20 min on ice in EMSA buffer (50 mM NaCl, 75 mM KCl, 25 mM Tris [pH 8], 13% glycerol, and 0.015% ×100). Samples were run on 4% (Figure S1C) or 6% (Figure S1D) polyacrylamide gels in 0.5× TBE buffer and imaged using a Typhoon (GE).

smFRET Assays

smFRET assays and analysis were performed as described previously (Reid et al., 2015, 2017). Briefly, NHEJ reactions composed of 50 nM Ku, LX, XLF gloxy (0.5 mg/mL glucose oxidase and 0.4 μg/mL catalase), and 1 nM dsDNA were added stepwise to NEB4 (20 mM TricAc [pH 7.5], 50 mM KAc, and 10 mM MgAc) supplemented with 0.8% glucose, ~5 mM Trolox, 1 mg/mL BSA, and 2 mM DTT. The reaction was immediately flowed into an imaging chamber that had been prepared with surface dsDNA (~250 pM). Movies consisting of 1,000 frames (33 Hz) were acquired for analysis of PECs. Trajectory analysis, histogram assembly, and autocorrelation of PECs were performed in MATLAB (Reid et al., 2017). Oligonucleotides used in smFRET experiments are detailed in Table S1.

Cell Lines

LIG4$^{-/-}$ cells were generated from parental HCT116 human colorectal cancer cells by conventional gene targeting and were the gift of Dr. Eric Hendrickson (Oh et al., 2013). We generated additional variants of the parental cells by CRISPR/Cas9 gene targeting. We introduced by electroporation plasmids to express Cas9 (Addgene 44758; Shen et al., 2013; 5 μg) and an sgRNA (Addgene 51133; Shen et al., 2014; 5 μg; guide sequence described in Table S1) that targets insert1-encoding sequence from wild-type *LIG4*, as well as a gene-targeting donor plasmid. The donor plasmid was engineered such that it contains 1.1 kb of sequence identical to the LIG4 gene, except as modified such that gene targeting ablates the small guide RNA (sgRNA) target site, generates the *LIG4*$^{\Delta i}$ mutation as described in Figure 1A, and introduces synonymous mutations that result in a BsmFI site used for screening. The native *LIG4* sequence in this region and resulting *LIG4*$^{\Delta i}$ alleles are described in Figure S3 and Table S1. Targeted puromycin-resistant clones were identified by amplification of the insert1 region using primers specific to the native locus (i.e., originate outside of donor sequence identity). Two independently generated clones, *LIG4*$^{\Delta i/\Delta i}$ a and b, were produced that possessed only targeted alleles after sequencing (Figure S3A). To generate *LIG4*$^{+r/+r}$ reverted cells we repeated gene targeting but started with *LIG4*$^{\Delta i/\Delta i}$ a cells and used an sgRNA specific for the *LIG4*$^{\Delta i}$ allele (Table S1) as well as a gene-targeting donor with wild-type sequence in this region. We verified LIG4 expression in all of these cell lines using standard western blot techniques (Figure S3B) and antibodies against human LIG4 (Serotec catalog no. AHP554) and human Ku70 (Abcam catalog no. ab62820). All 5 cell lines were cultured in McCoy's 5A medium (Corning) with 10% fetal bovine serum (Sigma) and determined to be free of mycoplasma contamination by PCR (Uphoff and Drexler, 1999); we additionally employed a third party to validate the absence of mycoplasma by an alternate method for a randomly selected cell line (Hoechst staining; Battaglia et al., 1980).

Cellular NHEJ Assays

Extrachromosomal DNA substrates described above (20 ng) were electroporated into 2 × 10^5 cells with pMAX-GFP plasmid (600 ng) at 1,350 V in one 30-ms pulse in 10 μL (Neon, Invitrogen). Transfected cells were incubated for 30 min in antibiotic-free McCoy's 5A media with 10% fetal bovine serum. Cellular repair products were harvested using a QIAamp DNA mini kit (QIAGEN). Each electroporation was reproduced in triplicate from 3 independent preparations of cells. Repair efficiency was quantified by qPCR as described above for in vitro joining assays.

Repair product structures were determined by restriction digest for the 8-oxoguanine (2-amino-7,9-dihydro-1*H*-purine-6,8-dione; Go) substrate and by high-throughput sequencing for all other substrates. For the Go substrate, harvested repair products were amplified with Cy5-labeled primers (Table S1) and digested with BstZ17I (New England Biolabs; recognizes transversion mutation after amplification of Go) and BamHI (New England Biolabs; recognizes accurately amplified Go) to identify directly ligated products. The intensities of digested and undigested bands were quantified using ImageJ.

To determine repair product structures of all other substrates, sequencing libraries were prepared by PCR amplification of repair products with primers containing 6-nt indices on their 5′ ends (Table S1). Amplified DNA (40 ng per library) was pooled into groups of 8–12 libraries, 5′ phosphorylated, and treated with Klenow exo- (NEB) to add dA to the 3′ termini. Ends were ligated to adapters for paired-end sequencing (Illumina). Pooled libraries were purified from 3% agarose gels to remove unligated adapters using the QIAquick gel extraction kit (QIAGEN). Recovered samples were amplified for an additional 9 cycles using enrichment primers (Illumina). Products were again purified using Ampure XP beads (Beckman Coulter). 27.27 ng from each of the 11 pools was combined (for a total of 300 ng of sample), supplemented with PhiX174 (40% final concentration), and submitted to the UNC high-throughput sequencing facility for a 2 × 75-bp MiSeq run (Illumina). Genomics Workbench was used to remove PhiX174 DNA, merge read pairs, de-index libraries, and remove low-quality sequences (CLC-Bio). Remaining sequences were analyzed using Microsoft Excel.

Colony-Formation and Cell Growth Assays

For colony-formation assays, seeding densities were determined independently for each dose and cell line such that 50–150 colonies would be

produced per 10-cm dish. Cells were plated on 10-cm dishes in fresh McCoy's 5A media with 10% fetal bovine serum, incubated for 4 hr, and then irradiated with indicated doses of X-rays using an RS 2000 irradiator (Rad Source Technologies). Colonies formed after 14 days were stained with a solution of crystal violet (0.5%) and glutaraldehyde (6%). Colonies were manually counted on three plates per dose and cell line. The surviving fraction of *LIG4*$^{-/-}$ cells treated with 3 Gy of X-rays was much less than 10^{-3}, and was excluded from analysis because the resulting faint, small colonies could not be reliably discriminated above background debris staining.

For live cell imaging, 2,000 cells were plated into 96-well plates in triplicate for each dose and cell line. After overnight incubation, cells were irradiated or treated with etoposide and placed into the IncuCyte live cell imager (Essen Biosciences). Four 215-mm^2 images were taken per well using 10× objective every 4 hr for a total of 120 hr. The confluence of each image was determined by generating a confluence mask with IncuCyte software (Essen Biosciences).

Statistical Analysis

For all experiments, means were tested for significance against a control (e.g., LIG4^{WT}, *LIG4*$^{+/+}$ cells) using two-tailed t tests for single comparisons, one-way ANOVA for multiple comparisons, and two-way ANOVA for comparisons with multiple variables. Dunnett's correction for testing multiple hypotheses was applied as necessary. For each experiment, the value and definition of n, the representation of error bars, the specific tests used, the specific control tested, and the determination of statistical significance are described in the figure legends.

SUPPLEMENTAL INFORMATION

Supplemental Information includes Supplemental Experimental Procedures, five figures, and one table and can be found with this article online at http://dx.doi.org/10.1016/j.celrep.2017.08.091.

AUTHOR CONTRIBUTIONS

M.P.C., D.A. Reid, E.R., and D.A. Ramsden prepared the manuscript and designed the experiments described therein. Experiments were performed by M.P.C., D.A. Reid, G.W.S., M.R.L., H.H.C., and G.W. Data were analyzed by M.P.C., D.A. Reid, E.R., and D.A. Ramsden.

ACKNOWLEDGMENTS

We thank Kaitlyn Walsh for performing experiments related to this work. We thank Dr. Eric Hendrickson for providing *LIG4*$^{+/+}$ and *LIG4*$^{-/-}$ cell lines used in this work. M.P.C. was supported by the National Cancer Institute (F31CA203156) and the National Institute of General Medical Sciences (T32GM007092). M.P.C., D.A. Ramsden, and G.W.S. were supported by the National Cancer Institute (CA084442). E.R. and D.A. Reid were supported by the National Institute of General Medical Sciences (GM108118). M.R.L., H.H.C., and G.W.S. were supported by the National Cancer Institute (CA100504) and the National Institute of General Medical Sciences (GM118009).

Received: July 19, 2017
Revised: August 22, 2017
Accepted: August 25, 2017
Published: September 19, 2017

REFERENCES

Andres, S.N., Modesti, M., Tsai, C.J., Chu, G., and Junop, M.S. (2007). Crystal structure of human XLF: a twist in nonhomologous DNA end-joining. Mol. Cell *28*, 1093–1101.

Andres, S.N., Vergnes, A., Ristic, D., Wyman, C., Modesti, M., and Junop, M. (2012). A human XRCC4-XLF complex bridges DNA. Nucleic Acids Res. *40*, 1868–1878.

Battaglia, M.F., Balducci, L., and Finocchiaro, M. (1980). Use of Hoechst 33258 fluorochrome for detection of mycoplasma contamination in cell cultures: development of a technique based on simultaneous fixation and staining. Boll. Ist. Sieroter. Milan. *59*, 155–158.

Biasini, M., Bienert, S., Waterhouse, A., Arnold, K., Studer, G., Schmidt, T., Kiefer, F., Gallo Cassarino, T., Bertoni, M., Bordoli, L., and Schwede, T. (2014). SWISS-MODEL: modelling protein tertiary and quaternary structure using evolutionary information. Nucleic Acids Res. *42*, W252–W258.

Breen, A.P., and Murphy, J.A. (1995). Reactions of oxyl radicals with DNA. Free Radic. Biol. Med. *18*, 1033–1077.

Budman, J., Kim, S.A., and Chu, G. (2007). Processing of DNA for nonhomologous end-joining is controlled by kinase activity and XRCC4/ligase IV. J. Biol. Chem. *282*, 11950–11959.

Chang, H.H.Y., Watanabe, G., Gerodimos, C.A., Ochi, T., Blundell, T.L., Jackson, S.P., and Lieber, M.R. (2016). Different DNA end configurations dictate which NHEJ components are most important for joining efficiency. J. Biol. Chem. *291*, 24377–24389.

Cotner-Gohara, E., Kim, I.-K., Hammel, M., Tainer, J.A., Tomkinson, A.E., and Ellenberger, T. (2010). Human DNA ligase III recognizes DNA ends by dynamic switching between two DNA-bound states. Biochemistry *49*, 6165–6176.

Cottarel, J., Frit, P., Bombarde, O., Salles, B., Négrel, A., Bernard, S., Jeggo, P.A., Lieber, M.R., Modesti, M., and Calsou, P. (2013). A noncatalytic function of the ligation complex during nonhomologous end joining. J. Cell Biol. *200*, 173–186.

Davis, B.J., Havener, J.M., and Ramsden, D.A. (2008). End-bridging is required for pol mu to efficiently promote repair of noncomplementary ends by nonhomologous end joining. Nucleic Acids Res. *36*, 3085–3094.

Ellenberger, T., and Tomkinson, A.E. (2008). Eukaryotic DNA ligases: structural and functional insights. Annu. Rev. Biochem. *77*, 313–338.

Gómez-Herreros, F., Romero-Granados, R., Zeng, Z., Alvarez-Quilón, A., Quintero, C., Ju, L., Umans, L., Vermeire, L., Huylebroeck, D., Caldecott, K.W., et al. (2013). TDP2-dependent non-homologous end-joining protects against topoisomerase II-induced DNA breaks and genome instability in cells and in vivo. PLoS Genet. *9*, e1003226.

Greco, G.E., Matsumoto, Y., Brooks, R.C., Lu, Z., Lieber, M.R., and Tomkinson, A.E. (2016). SCR7 is neither a selective nor a potent inhibitor of human DNA ligase IV. DNA Repair (Amst.) *43*, 18–23.

Gu, J., Lu, H., Tsai, A.G., Schwarz, K., and Lieber, M.R. (2007). Single-stranded DNA ligation and XLF-stimulated incompatible DNA end ligation by the XRCC4-DNA ligase IV complex: influence of terminal DNA sequence. Nucleic Acids Res. *35*, 5755–5762.

Ma, Y., Pannicke, U., Schwarz, K., and Lieber, M.R. (2002). Hairpin opening and overhang processing by an Artemis/DNA-dependent protein kinase complex in nonhomologous end joining and V(D)J recombination. Cell *108*, 781–794.

Mehta, A., and Haber, J.E. (2014). Sources of DNA double-strand breaks and models of recombinational DNA repair. Cold Spring Harb. Perspect. Biol. *6*, a016428.

Nair, P.A., Nandakumar, J., Smith, P., Odell, M., Lima, C.D., and Shuman, S. (2007). Structural basis for nick recognition by a minimal pluripotent DNA ligase. Nat. Struct. Mol. Biol. *14*, 770–778.

Nick McElhinny, S.A., Snowden, C.M., McCarville, J., and Ramsden, D.A. (2000). Ku recruits the XRCC4-ligase IV complex to DNA ends. Mol. Cell. Biol. *20*, 2996–3003.

Nick McElhinny, S.A., Havener, J.M., Garcia-Diaz, M., Juárez, R., Bebenek, K., Kee, B.L., Blanco, L., Kunkel, T.A., and Ramsden, D.A. (2005). A gradient of template dependence defines distinct biological roles for family X polymerases in nonhomologous end joining. Mol. Cell *19*, 357–366.

Nitiss, J.L. (2009). Targeting DNA topoisomerase II in cancer chemotherapy. Nat. Rev. Cancer *9*, 338–350.

Ochi, T., Wu, Q., Chirgadze, D.Y., Grossmann, J.G., Bolanos-Garcia, V.M., and Blundell, T.L. (2012). Structural insights into the role of domain flexibility in human DNA ligase IV. Structure *20*, 1212–1222.

Ochi, T., Gu, X., and Blundell, T.L. (2013). Structure of the catalytic region of DNA ligase IV in complex with an Artemis fragment sheds light on double-strand break repair. Structure *21*, 672–679.

Ochi, T., Blackford, A.N., Coates, J., Jhujh, S., Mehmood, S., Tamura, N., Travers, J., Wu, Q., Draviam, V.M., Robinson, C.V., et al. (2015). PAXX, a paralog of XRCC4 and XLF, interacts with Ku to promote DNA double-strand break repair. Science *347*, 185–188.

Oh, S., Wang, Y., Zimbric, J., and Hendrickson, E.A. (2013). Human LIGIV is synthetically lethal with the loss of Rad54B-dependent recombination and is required for certain chromosome fusion events induced by telomere dysfunction. Nucleic Acids Res. *41*, 1734–1749.

Pascal, J.M., O'Brien, P.J., Tomkinson, A.E., and Ellenberger, T. (2004). Human DNA ligase I completely encircles and partially unwinds nicked DNA. Nature *432*, 473–478.

Pryor, J.M., Waters, C.A., Aza, A., Asagoshi, K., Strom, C., Mieczkowski, P.A., Blanco, L., and Ramsden, D.A. (2015). Essential role for polymerase specialization in cellular nonhomologous end joining. Proc. Natl. Acad. Sci. USA *112*, E4537–E4545.

Reid, D.A., Keegan, S., Leo-Macias, A., Watanabe, G., Strande, N.T., Chang, H.H., Oksuz, B.A., Fenyo, D., Lieber, M.R., Ramsden, D.A., and Rothenberg, E. (2015). Organization and dynamics of the nonhomologous end-joining machinery during DNA double-strand break repair. Proc. Natl. Acad. Sci. USA *112*, E2575–E2584.

Reid, D.A., Conlin, M.P., Yin, Y., Chang, H.H., Watanabe, G., Lieber, M.R., Ramsden, D.A., and Rothenberg, E. (2017). Bridging of double-stranded breaks by the nonhomologous end-joining ligation complex is modulated by DNA end chemistry. Nucleic Acids Res. *45*, 1872–1878.

Roberts, S.A., Strande, N., Burkhalter, M.D., Strom, C., Havener, J.M., Hasty, P., and Ramsden, D.A. (2010). Ku is a 5′-dRP/AP lyase that excises nucleotide damage near broken ends. Nature *464*, 1214–1217.

Roth, D.B., Menetski, J.P., Nakajima, P.B., Bosma, M.J., and Gellert, M. (1992). V(D)J recombination: broken DNA molecules with covalently sealed (hairpin) coding ends in scid mouse thymocytes. Cell *70*, 983–991.

Roy, S., de Melo, A.J., Xu, Y., Tadi, S.K., Négrel, A., Hendrickson, E., Modesti, M., and Meek, K. (2015). XRCC4/XLF interaction is variably required for DNA repair and is not required for ligase IV stimulation. Mol. Cell. Biol. *35*, 3017–3028.

Shen, B., Zhang, J., Wu, H., Wang, J., Ma, K., Li, Z., Zhang, X., Zhang, P., and Huang, X. (2013). Generation of gene-modified mice via Cas9/RNA-mediated gene targeting. Cell Res. *23*, 720–723.

Shen, B., Zhang, W., Zhang, J., Zhou, J., Wang, J., Chen, L., Wang, L., Hodgkins, A., Iyer, V., Huang, X., and Skarnes, W.C. (2014). Efficient genome modification by CRISPR-Cas9 nickase with minimal off-target effects. Nat. Methods *11*, 399–402.

Tomkinson, A.E., Howes, T.R.L., and Wiest, N.E. (2013). DNA ligases as therapeutic targets. Transl. Cancer Res. *2*, 1219.

Tsai, C.J., Kim, S.A., and Chu, G. (2007). Cernunnos/XLF promotes the ligation of mismatched and noncohesive DNA ends. Proc. Natl. Acad. Sci. USA *104*, 7851–7856.

Uphoff, C.C., and Drexler, H.G. (1999). Detection of mycoplasma contaminations in cell cultures by PCR analysis. Hum. Cell *12*, 229–236.

Waters, C.A., Strande, N.T., Wyatt, D.W., Pryor, J.M., and Ramsden, D.A. (2014a). Nonhomologous end joining: a good solution for bad ends. DNA Repair (Amst.) *17*, 39–51.

Waters, C.A., Strande, N.T., Pryor, J.M., Strom, C.N., Mieczkowski, P., Burkhalter, M.D., Oh, S., Qaqish, B.F., Moore, D.T., Hendrickson, E.A., and Ramsden, D.A. (2014b). The fidelity of the ligation step determines how ends are resolved during nonhomologous end joining. Nat. Commun. *5*, 4286.

Wilson, T.E., Grawunder, U., and Lieber, M.R. (1997). Yeast DNA ligase IV mediates non-homologous DNA end joining. Nature *388*, 495–498.

Xing, M., Yang, M., Huo, W., Feng, F., Wei, L., Jiang, W., Ning, S., Yan, Z., Li, W., Wang, Q., et al. (2015). Interactome analysis identifies a new paralogue of XRCC4 in non-homologous end joining DNA repair pathway. Nat. Commun. *6*, 6233.